



# Universal and facile sol-gel approach for fabrication of multitudinous yolk-shell architectures

Hongqing Li<sup>1</sup> · Wenqi Xu<sup>1</sup> · Jiaqi Xu<sup>1</sup> · Mengxuan Zhu<sup>1</sup> · Rui Wang<sup>1</sup> · Heng Jiang<sup>1</sup> · Changzi Jin<sup>1</sup>

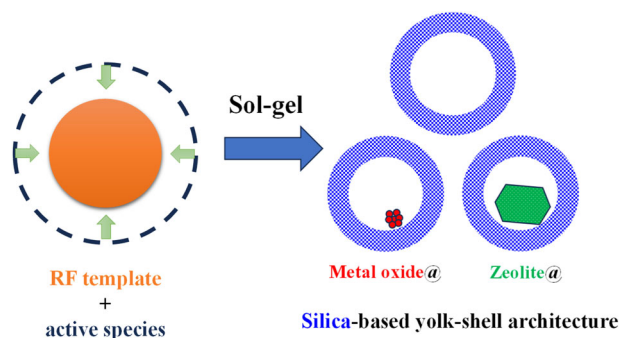
Received: 11 September 2023 / Accepted: 1 December 2023 / Published online: 19 December 2023

© The Author(s), under exclusive licence to Springer Science+Business Media, LLC, part of Springer Nature 2023

## Abstract

The nanoreactors with yolk-shell configuration have been one of the most attractive objects because of their unique performance in specific reactions. However, complicated synthesis procedures have restricted the truth understanding and wide application of the yolk-shell architectures. This article presents a universal and facile sol-gel process for fabrication of mesoporous silica hollow structure and derived yolk-shell composites with extended Stöber resorcinol-formaldehyde resin as sacrificed template. The crucial influence factors for the morphology of products are investigated. A series of yolk-shell composites with multitudinous components have been successfully designed and are further catalytic tested by different reactions. This work has provided a universal avenue for the fabrication of yolk-shell nanoreactors to suit specific reaction needs.

## Graphical Abstract



**Keywords** Yolk-shell architecture · Sol-gel · Resorcinol-formaldehyde resin · Template · Catalysis

## Highlights

- The resorcinol-formaldehyde resin is an effective template to construct hollow mesoporous silica.
- Suitable surfactant ligand and solvent composition are crucial.
- Universal yolk-shell architecture can be fabricated by this facile approach.

## 1 Introduction

Rational design of nanocomposites with unique architecture is significant to display the promising properties of materials and to achieve their full potential in diverse applications [1–6]. The yolk-shell architecture is a typical hybrid generally consisting of movable core encapsulated in

✉ Changzi Jin  
jin\_chz@163.com

<sup>1</sup> School of Petrochemical Engineering, Liaoning Petrochemical University, Fushun 113001, China

heterogeneous hollow outer shell, which is also called rattle-type structure [7–9]. Compared with conventional core-shell and other architecture, the yolk-shell systems usually possess the features of low density, large surface area, unique interior space and enhanced loading capacity. Over the past few decades, the controlled preparation, structural characterization and application of yolk-shell nanocomposites have attracted much attention [10–20]. Among those reported yolk-shell materials, silica-based analogs are undoubtedly one of the most popular objects for their prominent features, such as adjustable porous structure, abundant porosities, excellent stability and biocompatibility, which are widely used in the field of catalysis, drug storage and delivery [8, 21–30].

To date, the developed preparation strategy for yolk-shell silica-based composites mainly include template-assisted (hard- and soft-template) and template-free (post-treatment of selective etching) method, which have their own advantage and disadvantage. For the so-called hard-template approach, a core-shell hybrid with easily removable inner shell should be pre-fabricated. After the removal of the sacrificed inner shell template, the well-defined yolk-shell architecture is obtained [8, 21, 22]. By contrast, the soft-template method is simplified process, in which the core materials are directly covered by hollow silica shell with assistance of special surfactants [31]. However, only a small minority of the surfactants are effective to synthesize yolk-shell composites and it is difficult to adjust the structural parameters of the final products. Different from the aforementioned synthesis approaches, the post etching strategy to construct yolk-shell architecture does not depend on the presence of template. With the etching effect of specific solvent, both the core materials and silica shells can be partial dissolved into hollow cavity of yolk-shell architecture. Especially the silica shells from sol-gel (Stöber) process, which are chemically inhomogeneous and can be selective etched by basic solution or even the hot water [27, 32, 33]. Although the post-etching strategy avoids using templates, the synthesis conditions are not easy to control and the porosities and surface areas of silica shells in final products are relative scarce. Therefore, the hard-template method is the most attractive approach to fabricate the well-defined and adjustable yolk-shell architecture composites regardless of its multistep procedure nature.

Carbonaceous materials are known as the most widely adopted hard-templates for constructing hollow cavity of yolk-shell structure, which can be removed easily through calcination under air atmosphere [8, 22]. In order to obtain the well-defined yolk-shell silica-based composites, the regular shaped carbonaceous-based intermediates should be prepared first. In addition, an adequate interaction between silica shells and carbonaceous template is necessary, so that the silica shells can successfully cover onto the templates.

Since Liu et al. [34] had developed the Stöber system to the synthesis of resorcinol-formaldehyde (RF) resin and corresponding carbon spheres, many carbonaceous composites with well-defined yolk-shell architecture have been facilely prepared through this so-called extended Stöber method with silica as hard-template [35–38]. Although generated from similar system of EtOH-H<sub>2</sub>O-NH<sub>3</sub>, both silica gel and RF resin possess same negatively charged surface. Therefore, a positive charged surface modification is usually necessary to improve the interaction between silica and RF resin, and the cationic surfactant is demonstrated to be very effective for the induction of RF resin coating over other materials [36, 37, 39]. We had systematically investigated the effect of surface modifier on RF resin coating over Stöber silica spheres in previous report [39]. Herein, we investigate the silica-coating behavior over extended Stöber RF resin, and further fabricate the silica-based yolk-shell composites through sol-gel process. The catalytic performance of prepared multitudinous yolk-shell composites is tested in different reactions.

## 2 Experimental

### 2.1 Chemicals

Tetraethylorthosilicate (TEOS), cetyltrimethylammonium bromide (CTAB), resorcinol, formaldehyde aqueous solution (40 wt %), tetradecyltrimethylammonium bromide (TTAB), dodecylamine (DDA), nitrobenzene and o-chloronitrobenzene were purchased from Shanghai Aladdin Biochemical Technology Co., Ltd. Methanol, ethanol, hydrogen peroxide (H<sub>2</sub>O<sub>2</sub>, 30 wt%) and ammonia hydroxide (NH<sub>3</sub>·H<sub>2</sub>O, 25–28 wt %) were purchased from Tianjin Kermel Chemical Co. Chloroplatinic acid hydrate (H<sub>2</sub>PtCl<sub>6</sub>·6H<sub>2</sub>O), hexachloroiridium acid hydrate (H<sub>2</sub>IrCl<sub>6</sub>·6H<sub>2</sub>O), tetrabutylorthotitanate (TBOT), thiophene, ferric acetylacetonate (Fe(acac)<sub>3</sub>) and tetrapropylammonium hydroxide (TPAOH, 25 wt%) were purchased from Beijing Innochem Science and Technology Ltd. The distilled water was homemade. All chemicals were of analytical grade and used as received without any purification.

### 2.2 Synthesis of materials

#### 2.2.1 RF resin spheres

The RF resin spheres with uniform diameters were synthesized by the reported extended Stöber method [34]. Typically, deionized water (60 mL), ethanol (15 mL), and NH<sub>3</sub>·H<sub>2</sub>O (0.3 mL) were mixed together, followed by the addition of 0.2 g resorcinol and 0.3 mL formaldehyde solution. Then, the mixture was further stirred for 24 h. The

solid product was collected by centrifugation and washed with ethanol and water for several times and dried at 100 °C.

### 2.2.2 Hollow mesoporous silica spheres

Hollow mesoporous silica was prepared through sol-gel process with the obtained RF resin spheres as hard template. Typically, 0.2 g RF resin spheres was dispersed in 80 mL water/ethanol mixed solvent (volume ratio at 5/3). With the addition of 0.106 g CTAB and 2.0 mL  $\text{NH}_3\cdot\text{H}_2\text{O}$ , the obtained mixture was ultrasound-treated for 30 min. Then, 0.57 g of TEOS was dropwise into the synthetic system under stirring. The stirring was maintained at 40 °C for 18 h, and the product was collected by centrifugation and washed with ethanol and water for several times. After dried at 100 °C, the sample was calcined at 550 °C for 5 h under air atmosphere to remove the organic components. Finally, the mesoporous silica hollow spheres, denoted as H-mSiO<sub>2</sub>, were obtained.

### 2.2.3 Yolk-shell MO<sub>x</sub>-mesoporous silica composites

To prepare the yolk-shell composites, the introduction of precursors of core materials to the synthetic system is important. In detail, 0.2 g RF resin spheres and 0.186 g  $\text{H}_2\text{PtCl}_6$  aqueous solution (38.6 mM) were added in 50 mL water and the mixture was reflux at 80 °C for 24 h to allow the adsorption of  $\text{H}_2\text{PtCl}_6$  molecules on the surface of template. After centrifugation, the resultant Pt-containing RF resin spheres were redispersed in water/ethanol and undergone mesoporous silica coating process and the subsequent drying and calcination treatment through similar procedures described above. The obtained yolk-shell PtO<sub>x</sub>-mesoporous silica composite was denoted as PtO<sub>x</sub>@H-mSiO<sub>2</sub>.

The preparation process for IrO<sub>x</sub>@H-mSiO<sub>2</sub> and FeO<sub>x</sub>@H-mSiO<sub>2</sub> are similar to PtO<sub>x</sub>@H-mSiO<sub>2</sub> except that the core precursors of  $\text{H}_2\text{PtCl}_6$  were replaced by  $\text{H}_2\text{IrCl}_6$  and Fe(acac)<sub>3</sub>, respectively.

### 2.2.4 Yolk shell micro/mesoporous titanium-silica

Firstly, microporous titanosilicate zeolite (TS-1) was synthesized according to previous reports [40]. TEOS and TBOT were used as silicon and titanium source, respectively and were mixed with the template of TPAOH to form the reaction mixture with composition of SiO<sub>2</sub>:0.025TiO<sub>2</sub>:0.295TPAOH:38H<sub>2</sub>O. After crystallization at 170 °C for 48 h, the zeolite product was collected by centrifugation and dried at 100 °C and calcined at 550 °C for 5 h to remove the template. Thus, the nano-sized TS-1 was obtained.

Then, the calcined TS-1 zeolite (0.25 g) was dispersed in 40 mL water and 20 mL ethanol containing 0.5 g CTAB and 0.3 mL  $\text{NH}_3\cdot\text{H}_2\text{O}$ . The mixture was treated by ultrasound for 30 min, followed by the addition of 0.1 g resorcinol and 0.15 mL formaldehyde solution under stirring. The final synthesis mixture was further stirred at room temperature for 24 h and the RF resin coating zeolite products (denoted as TS-1@RF) were collected by centrifugation and dried at 100 °C.

Finally, the TS-1@RF was further coated by mesoporous titanium-silica through similar sol-gel process to H-mSiO<sub>2</sub> with a little difference. 0.5 g TS-1@RF was used as starting material and 0.57 g TEOS together with 0.019 g TBOT were dropwise into synthesis mixture. After the routine separation, drying and calcination procedures, the yolk-shell microporous/mesoporous titanium-silica was obtained, denoted as TS-1@H-mTi-SiO<sub>2</sub>.

## 2.3 Selective hydrogenation of nitroarenes to amines

Selective hydrogenation of nitroarenes to corresponding amines was performed in a Teflon-lined autoclave. In brief, 5 mL of the solution of nitroarenes in ethanol (0.1 M) and 30 mg of the catalyst were added into the autoclave. It should be noted that the yolk-shell composites for catalytic tests and characterization were used without rigorous grinding to protect the integrality of architecture. Then, the autoclave was swept by H<sub>2</sub> several times to exclude the air and sealed with pressure at 0.3 MPa. The reaction mixture was stirred at 40 °C for 2 h and the reaction products were analyzed by means of GC PerkinElmer AutoSystem XL equipped with an Elite-5 capillary column and FID detector.

## 2.4 Oxidative desulfurization reaction

The sulfocompound Th and DBT were dissolved in octane to act as model oil (1000 ppm). For the oxidative desulfurization reaction, 10 mL model oil, 10 mL solvent (water for Th and methanol for DBT) and 100 mg catalysts were added in a three-neck glass flask. Then the oxidant H<sub>2</sub>O<sub>2</sub> (10 μL) was injected into the reactor and the reaction mixture was continuously stirred at 80 °C for 4–6 h. The oil phase was extracted periodically and analyzed on GC HP6890 equipped with HP-5 capillary column and FPD detector.

## 2.5 Characterization

Transmission electronic microscopy (TEM) images, scanning transmission electronic microscopy (STEM) and EDX element mapping analysis were taken on a JEM-2100 electronic microscope with an accelerating voltage of 200 kV. Scanning electronic microscopy (SEM) images were detected on a SU8010 field-emission scanning electronic microscope

operating at an accelerating voltage of 5–8 kV. Small- and wide- angle X-ray diffraction (XRD) pattern was recorded in a Bruck D8 Advance powder X-ray diffractometer using Cu K $\alpha$  radiation. Nitrogen physical adsorption/desorption isotherms were measured on Quantachrome Autosorb-IQ2-MP physical adsorption apparatus. The mesopore size distributions were calculated from the adsorption branches of the isotherms using the Barrett-Joyner-Halenda (BJH) model and the specific surface areas were calculated using the BET method. UV-vis spectra were obtained on JASCO UV550 spectrometer with BaSO<sub>4</sub> as the standard.

## 3 Results and discussion

### 3.1 Synthesis of H-mSiO<sub>2</sub> spheres

For the preparations of H-mSiO<sub>2</sub> through hard-template approaches, the choice of template is crucial, including the facile synthesis, regular and controllable shape and improvable interaction with silica shell. Compared to other carbonaceous spheres, the extended Stöber method for synthesize RF resin spheres is mild and efficient. Due to generating from same synthesis system, RF resin and silica have potential interaction each other and can in-situ form the core-shell structure even without special ligand [35, 38, 41]. Therefore, the RF resin is thought to be ideal candidate for constructing hollow silica architecture. Figure 1 presents the TEM images and small-angle XRD pattern of RF resin spheres and the prepared H-mSiO<sub>2</sub> spheres. Obviously, the RF resin spheres prepared by extended Stöber method possess uniform morphology with diameter of about 200 nm. With the assistance of CTAB, silicon oligomer from TEOS hydrolysis can assemble to form mesoporous silica layer over the RF resin spheres and further form the regular hollow sphere structure after removal of RF resin template (Fig. 1b). During this process, CTAB not only act as ligand to induce the silica species depositing onto the surface of RF resin spheres, but also as the mesopore template of silica shell. The HRTEM image clearly reveals the wormlike mesostructure of the silica shell of H-mSiO<sub>2</sub> spheres (Fig. 1c). The small-angle XRD pattern of H-mSiO<sub>2</sub> (Fig. 1d) displays single intense reflection at  $2\theta = 2.5^\circ$ , which indicates the lower order degree of wormlike mesostructured silica shell.

Cationic surfactants other than CTAB are also effective to construct hollow silica spheres. As showed in Fig. 2a, H-mSiO<sub>2</sub> can be synthesized by using TTAB with shorter alkyl chain as ligand and mesopore template. It was noting that our previous research has revealed that primary amine (DDA) cannot induce the RF resin layer deposit onto the surface of silica sphere, regardless of its positive charge effect [39]. However, one can find that H-mSiO<sub>2</sub> with wormlike

mesostructured shell has been obtained with DDA as ligand (Fig. 2b), which indicates the successful coating of mesoporous silica over RF resin spheres with assistance of DDA. The different behavior of DDA in two processes may be due to its different ways to participate in polymerizations of RF resin and silica. By comparison, CTAB-containing system produces H-mSiO<sub>2</sub> with uniform and regular morphology and is adopted in following research.

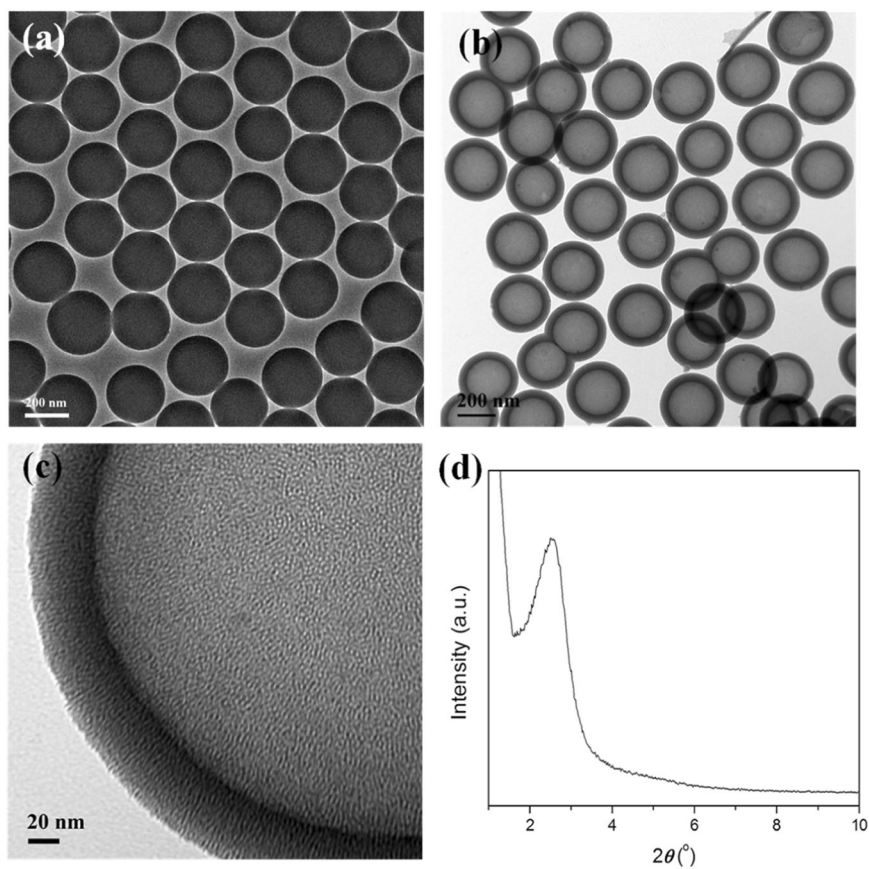
The sol-gel process for preparation of H-mSiO<sub>2</sub> adopts mixed solvent of water/ethanol system, which is also called modified Stöber process. The composition of solvent was demonstrated to be important during Stöber process in the previous researches [42]. Herein, the effect of solvent composition on the morphology of H-mSiO<sub>2</sub> products was investigated and the results are showed in Fig. 3. The typical synthesis of H-mSiO<sub>2</sub> use mixed solvent of water/ethanol with volume ratio at 5:3 and can produce uniform and regular hollow spheres (Figs. 1, 2). Reducing slightly the ethanol amount (water/ethanol volume ratio 3:1) does not change the morphology of H-mSiO<sub>2</sub> products (Fig. 3b). Although the organic solvent-free system is the objective for the synthesis of many materials, the products from entire water system do not exhibit spheric morphology but irregular hollow structure full of wrinkle (Fig. 3a). The formation of such morphology may be because only thin and discrete silicas deposit onto RF resin templates in the ethanol-free synthetic system. After the removal of templates, the hollow structure collapsed and shrank and formed irregular shaped architecture. However, the ethanol-rich mixed solvent (water/ethanol volume ratio 1:3) does not yield uniform hollow spheric products either, which are barely visible hollow structure consisting of discrete silica particles (Fig. 3c). Therefore, in order to obtain uniform and regular H-mSiO<sub>2</sub> products, water-dominant mixed solvent is necessary.

### 3.2 Fabrication of MO<sub>x</sub>@H-mSiO<sub>2</sub> yolk-shell composites

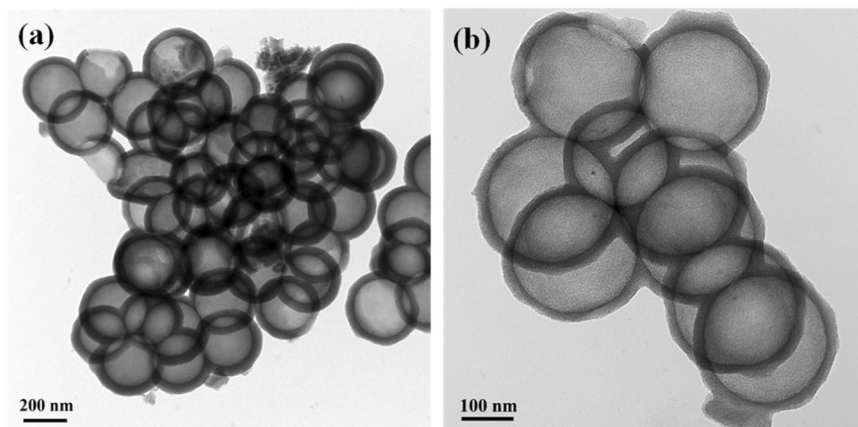
It is reasonable to expand this powerful synthesis approach to the fabrications of yolk-shell composites. Figure 4 presents the TEM, SEM, STEM and element mapping analysis for PtO<sub>x</sub>@H-mSiO<sub>2</sub> and related Pt-doped RF resin spheres. For the Pt-doped RF sample, it can be observed that there are some tiny particles on the surface of RF resin spheres (Fig. 4a), which indicates that the Pt-species has been doped into the template through hydrothermal treatment. With the covering of mesoporous silica shell and subsequent template-removal process, the final PtO<sub>x</sub>@H-mSiO<sub>2</sub> with yolk-shell architecture can be obtained. As the TEM image has shown (Fig. 4b), the clusters composed of many tiny particles are deposited on the inside of silica hollow spheres, which indicates that the high-temperature calcination and the removal of RF resin scaffold do not lead to



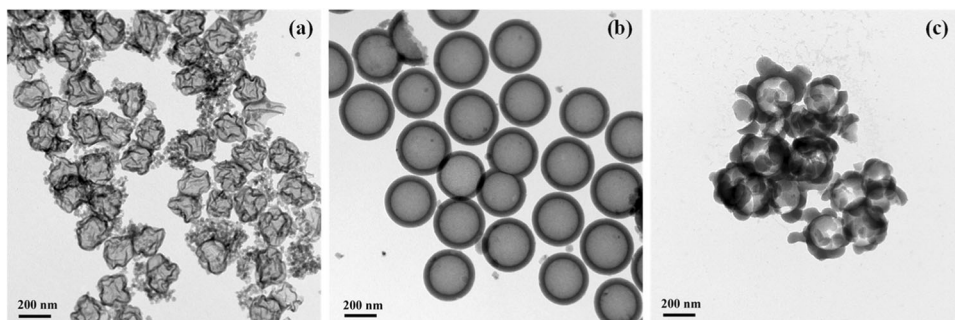
**Fig. 1** TEM images of RF resin sphere (a) and H-mSiO<sub>2</sub> (b), HRTEM (c) and small-angle XRD pattern of H-mSiO<sub>2</sub>



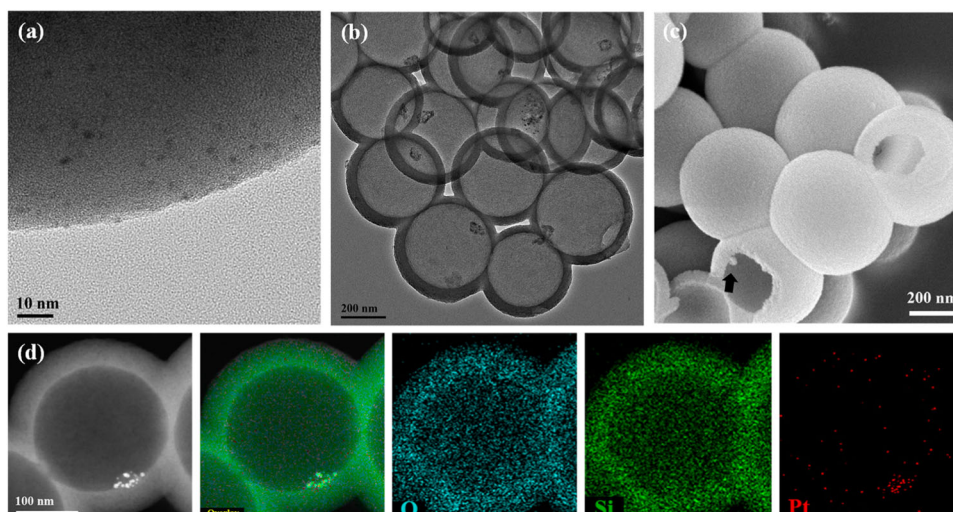
**Fig. 2** TEM images of H-mSiO<sub>2</sub> synthesized with assistance of (a) TTAB and (b) DDA



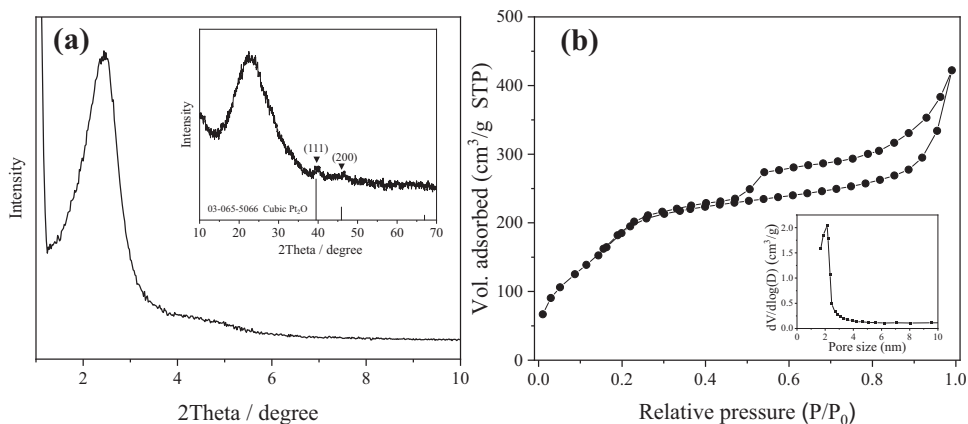
**Fig. 3** Products from mixed solvent with (a) entire water, (b) water/ethanol volume ratio 3:1 and (c) water/ethanol volume ratio 1:3



**Fig. 4** TEM images of (a) Pt-doped RF resin template and (b)  $\text{PtO}_x$ @H-mSiO<sub>2</sub>, (c) SEM and (d) dark filed STEM images of  $\text{PtO}_x$ @H-mSiO<sub>2</sub> and corresponding element mapping

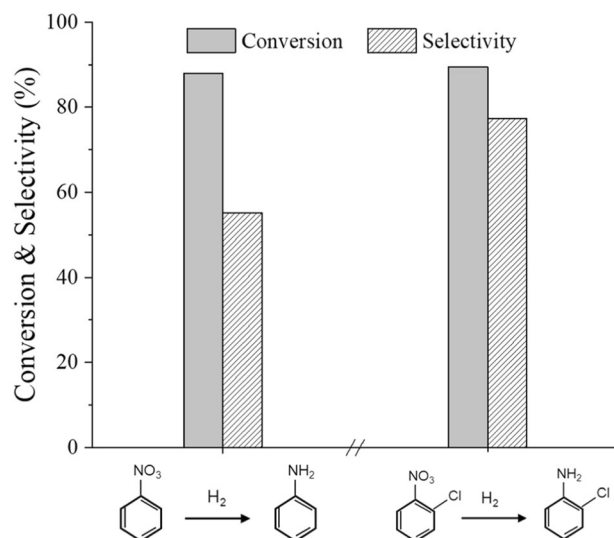


**Fig. 5** a Small and wide (inset) angle XRD patterns and (b) N<sub>2</sub> physical adsorption-desorption isotherm and BJH pore size distribution (inset) of  $\text{PtO}_x$ @H-mSiO<sub>2</sub>



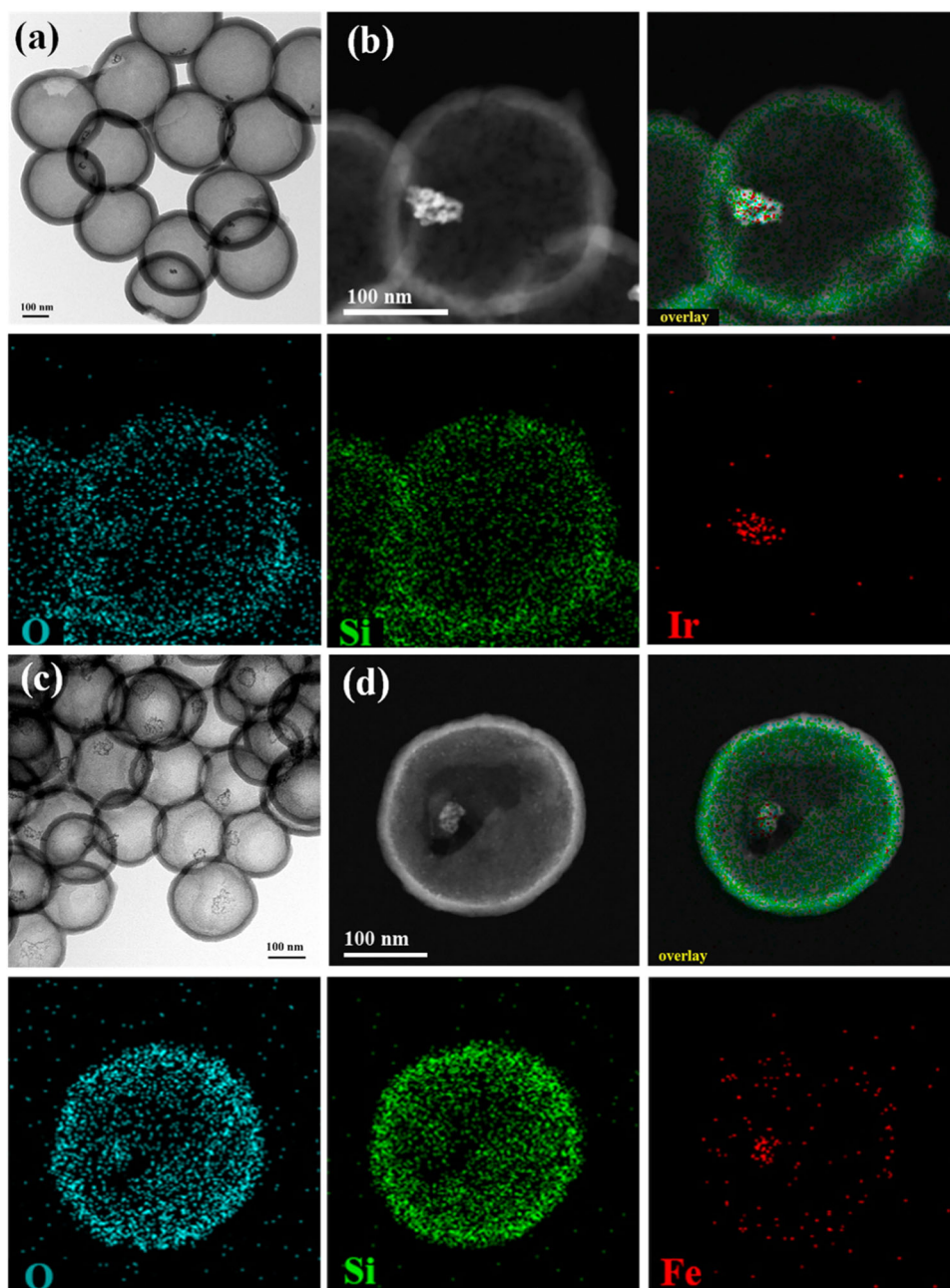
obvious sintering of  $\text{PtO}_x$  particles. The SEM image confirms the morphology of  $\text{PtO}_x$ @H-mSiO<sub>2</sub> more visually (Fig. 4c). Except the  $\text{PtO}_x$  particles in broken silica shell (Fig. 4c arrow), no metallic oxide particles can be found on the outer surface of silica shell. In addition, the STEM-EDX element mapping (Fig. 4d) show evenly distributed O and Si elements, whereas the Pt is mainly concentrated at the core particle within silica shell. These results also identify the yolk-shell architecture of  $\text{PtO}_x$ @H-mSiO<sub>2</sub> with metallic oxide particles encapsulated in mesoporous silica shell.

Figure 5 shows the small and wide angle XRD patterns and N<sub>2</sub> physical adsorption analysis of prepared  $\text{PtO}_x$ @H-mSiO<sub>2</sub>. Similar to the H-mSiO<sub>2</sub>, the small angle XRD pattern of  $\text{PtO}_x$ @H-mSiO<sub>2</sub> exhibits single diffraction peak at 2.4°, indicating the mesostructured silica shell. In wide angle region (Fig. 5a inset), besides the broad reflection of 20–25° assigning to amorphous silica, there are weak signal at  $2\theta = 39.5^\circ$  and  $46^\circ$ , which can be indexed to the (111) and (200) crystalline plane of cubic  $\text{Pt}_2\text{O}$  crystal (03-065-

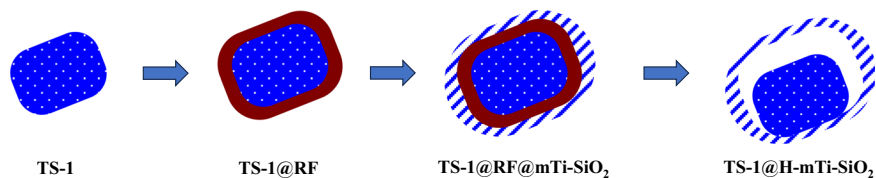


**Fig. 6** Catalytic performance of yolk-shell Pt@H-mSiO<sub>2</sub> in selective hydrogenation of nitrobenzene and *o*-nitrochlorobenzene

**Fig. 7** TEM images (a, c) and dark field STEM (b, d) of  $\text{IrO}_x@H\text{-mSiO}_2$  (a, b) and  $\text{FeO}_x@H\text{-mSiO}_2$  (c, d) and corresponding element mapping



**Fig. 8** The schematic representation of the synthesis of  $\text{TS-1}@H\text{-mTi-SiO}_2$



5066), respectively. The weak diffraction peak also indicates the absence of large platinum oxide particles. In addition, the mesoporous shell of  $\text{PtO}_x@H\text{-mSiO}_2$  is also confirmed by  $\text{N}_2$  physical adsorption-desorption isotherm (Fig. 5b). Obviously, the  $\text{PtO}_x@H\text{-mSiO}_2$  shows type-IV

isotherm with  $\text{N}_2$  uptake step at  $P/P_0$  of 0.2–0.25, suggesting the filling of  $\text{N}_2$  molecules in mesopores. The obvious hysteresis at  $P/P_0$  range of 0.6–1.0 can be due to the filling of  $\text{N}_2$  in cavity of mesoporous silica shells. The BJH pore size distribution (Fig. 5b inset) displays that the



**Fig. 9** TEM images of (a) TS-1, (b) TS-1@RF, (c) TS-1@H-mTi-SiO<sub>2</sub> and SEM image (d) of TS-1@H-mTi-SiO<sub>2</sub>. Inset: XRD pattern of TS-1

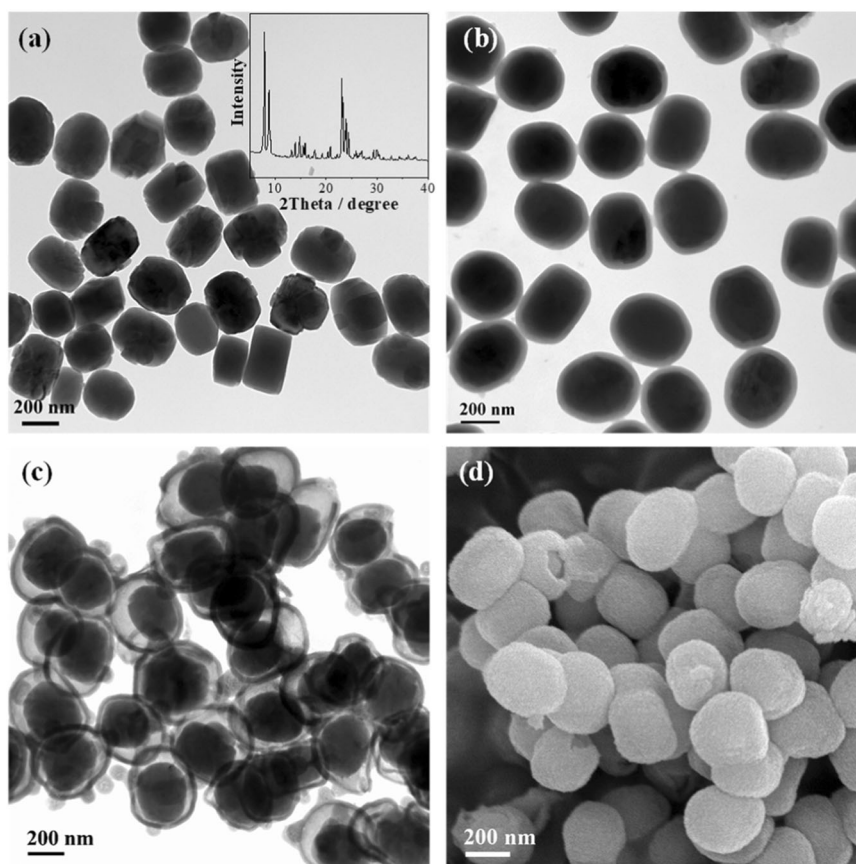
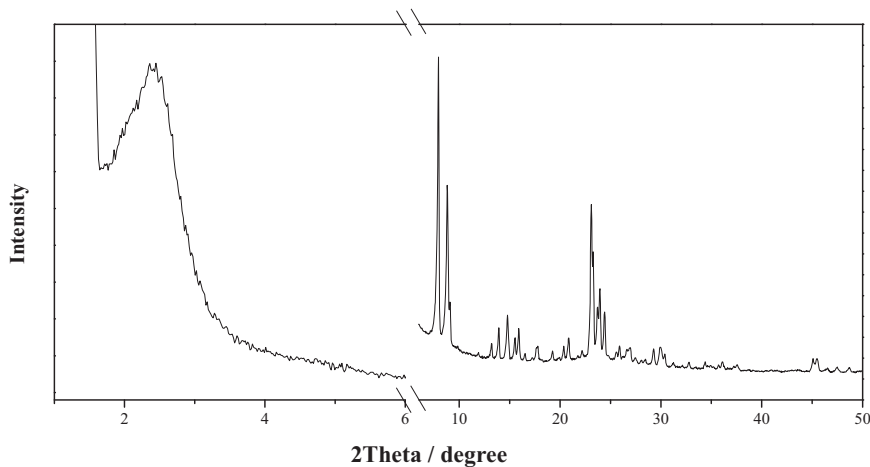


**Fig. 10** Small and wide angle XRD pattern of TS-1@H-mTi-SiO<sub>2</sub>



mesopore diameters of PtO<sub>x</sub>@H-mSiO<sub>2</sub> are centered at around 2.1 nm.

The PtO<sub>x</sub> nanoclusters encapsulated in permeable porous silica shell will be an ideal nanoreactor for heterogeneous catalysis. Herein, the catalytic rests for yolk-shell PtO<sub>x</sub>@H-mSiO<sub>2</sub> are performed in selective hydrogenation of nitroarenes to corresponding amines. The PtO<sub>x</sub>@H-mSiO<sub>2</sub> should be reduced by H<sub>2</sub> to metallic composite (Pt@H-mSiO<sub>2</sub>) before reactions. Fig. 6 presents the catalytic results of the

yolk-shell catalyst in selective hydrogenation of nitrobenzene and *o*-nitrochlorobenzene. It can be found that the yolk-shell catalyst exhibits similar activity in two reactions with conversion of about 90% and different selectivity for target product (58% for aniline and 77% for *o*-chloroaniline). The fabrication strategy for yolk-shell Pt-silica catalyst can be expanded into other composites. As Fig. 7 has shown, when the platinum precursor of H<sub>2</sub>PtCl<sub>6</sub> was replaced by H<sub>2</sub>IrCl<sub>6</sub> and Fe(acac)<sub>3</sub>, the IrO<sub>x</sub>@H-mSiO<sub>2</sub> and FeO<sub>x</sub>@H-mSiO<sub>2</sub> with



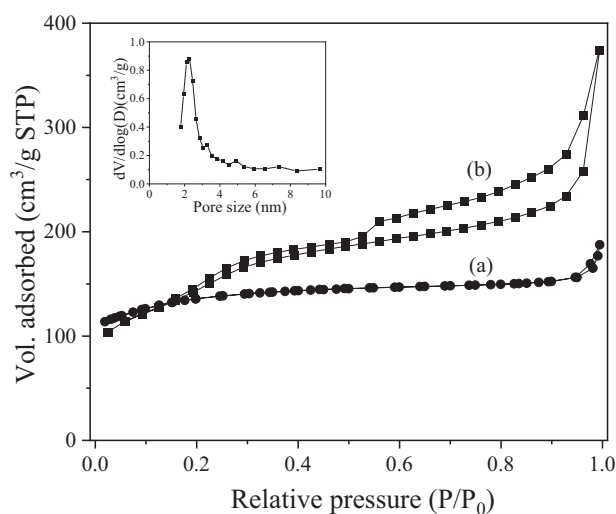


**Fig. 11**  $N_2$  physical adsorption-desorption isotherms of (a) TS-1 and (b) TS-1@H-mTi-SiO<sub>2</sub>. Inset: BJH pore size distribution of TS-1@H-mTi-SiO<sub>2</sub>

**Table 1** Textural properties of TS-1 and TS-1@H-mTi-SiO<sub>2</sub>

Sample	$d_{100}^a$ (nm)	$a_0^b$ (nm)	$S_{total}^c$ (m <sup>2</sup> /g)	$S_{micro}^d$ (m <sup>2</sup> /g)	$V_{total}^e$ (m <sup>3</sup> /g)	$V_{micro}^f$ (m <sup>3</sup> /g)	$D_{meso}^g$ (nm)
TS-1	--	--	476	453	0.29	0.20	--
TS-1@H-mTi-SiO <sub>2</sub>	3.7	4.3	523	381	0.58	0.19	2.2

<sup>a</sup> Calculated from XRD analysis. <sup>b</sup>  $a_0 = 2d/3^{1/2}$ . <sup>c</sup> Total surface area is calculated by BET method. <sup>d</sup> Microporous surface area is calculated from t-plot analysis. <sup>e</sup> Total pore volume is calculated from the volume adsorbed of P/P<sub>0</sub> at 0.99. <sup>f</sup> Microporous surface area is calculated from t-plot analysis. <sup>g</sup> Mesopore diameter is from BJH pore size distribution.

uniform similar yolk-shell architecture to PtO<sub>x</sub>@H-mSiO<sub>2</sub> were prepared, respectively. Therefore, targeted yolk-shell nanoreactors can be fabricated individually according to specific reaction needs.

### 3.3 Fabrication of yolk-shell micro/mesoporous titanium-silica

Combining of microporous zeolites and mesoporous materials serves to rectify the inadequate porosity and active site possessed by each component when it exists alone [43–45]. The synthesis strategy presented here is also applicable for fabrication of yolk-shell micro/mesoporous composites, which is schematically described in Fig. 8. Slightly different from the synthesis procedures described above, the preparation of core materials of microporous zeolites precedes that of RF resin template. The microporous TS-1 zeolite prepared through conventional hydrothermal process is used as starting material, whose TEM image and XRD pattern are

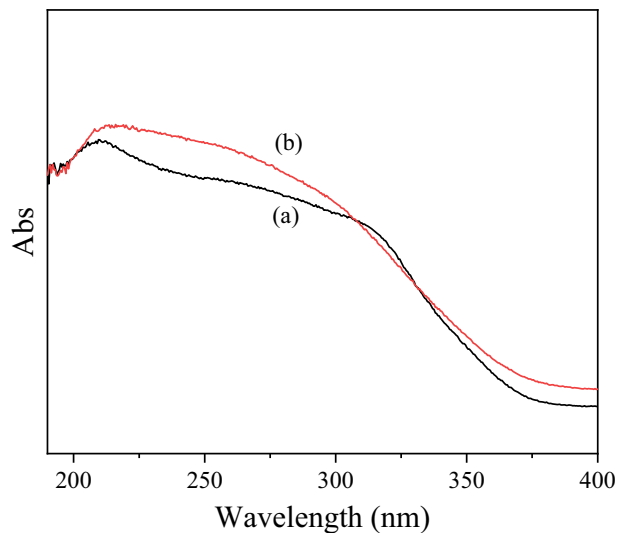
showed in Fig. 9. It can be observed that the prepared TS-1 zeolite is uniform monodispersed elliptical particles with dimension of 200 × 300 nm and possesses MFI structure with high crystallinity. Then, the TS-1 particles are coated by RF resin with assistance of CTAB through extended Stöber process and the uniform core-shell TS-1@RF has been obtained, as can be seen in TEM image in Fig. 9b. In the next step, the TS-1@RF is further coated with mesoporous shell through the similar approach described in Sections 3.1 and 3.2 with a little difference, namely the titanium species are incorporated in mesoporous shell. With the removal of RF resin layer, the yolk-shell micro/mesoporous composite with TS-1 zeolites encapsulating in mesoporous Ti-silica hollow spheres is obtained (Fig. 9c). Full view showed by SEM image also confirm the yolk-shell architecture of the composite and all the TS-1 crystals were coated by outer shell (Fig. 9d). The small and wide angle XRD pattern of TS-1@H-mTi-SiO<sub>2</sub> is showed in Fig. 10. The appearance of reflection in small angle region indicates the long-range order of mesostructure shell, while the strong diffraction peaks assigning to MFI topology confirm that TS-1 has been preserved well in the yolk-shell composite.

Figure 11 presents the  $N_2$  physical adsorption-desorption isotherms of TS-1 and TS-1@H-mTi-SiO<sub>2</sub> and relevant textural properties are listed in Table 1. Compared to the type-I isotherm of TS-1 zeolite, the yolk-shell composite exhibits combined type-I and type-IV isotherm. Besides the high  $N_2$  uptake at low relative pressure range, there is an obvious uptake step at P/P<sub>0</sub> of 0.2–0.3, indicating the existence of mesopores with uniform size. The abrupt increase of adsorption and hysteresis at high relative pressure region confirm the existence of hollow interior. The BJH pore size distribution of TS-1@H-mTi-SiO<sub>2</sub> further exhibits that the mesopores are centered at 2.2 nm (Table 1). The remarkably increased  $N_2$  uptake at high relative pressure may be related to the hollow structure. It is because the presence of mesoporous shell, the specific surface area and pore volume of TS-1@H-mTi-SiO<sub>2</sub> are greater than that of pure TS-1 zeolite (Table 1). The absorbance band at 210–220 nm in UV-vis analysis has identified the existence of framework Ti species in prepared materials (Fig. 12).

The research on desulfurization of fuel has certain value on the theory research and practical application [46–48]. Herein, the catalytic performance of the synthesized Ti-containing porous silica was tested in oxidations of organic sulfides and are showed in Fig. 13. For the oxidation of small molecule Th reactant, the microporous TS-1 zeolite is highly active and reaches the Th removal as high as more than 95% within 1 h, which is accordance with previous report. The yolk-shell TS-1@H-mTi-SiO<sub>2</sub> also exhibits high activity in Th

oxidation because of the fact that TS-1 particles are involved in the composite system. Without considering the reactant molecules accessibility, the Ti-containing mesoporous silica has no advantage over conventional microporous zeolites. Therefore, TS-1@H-mTi-SiO<sub>2</sub> is slightly inferior than TS-1 in Th oxidation. As to the bulky molecule DBT reaction, different from the absolutely inactive pure TS-1, the TS-1@H-mTi-SiO<sub>2</sub> exhibits

a certain activity with DBT removal of 64% after reaction 6 h, which indicates that the mesoporous Ti-containing silica shell contribute to catalyzing bulky molecule reaction. Therefore, this micro/mesoporous yolk-shell composite possess wide applicability compared to conventional TS-1 zeolite with mono-microporous channel. It is noted that the synthesis strategy for micro/mesoporous yolk-shell composite is universal and can be expanded to other yolk-shell counterparts. For example, the acid catalyst of H-β@H-mAl-SiO<sub>2</sub> can be fabricated through this protocol and is showed in Fig. 14. It is worth expecting that the composite catalytic system with complementary porosities and active sites will be outstanding in specific reactions.



**Fig. 12** UV-vis spectra of (a) TS-1 and (b) TS-1@H-mTi-SiO<sub>2</sub>

**Fig. 13** Oxidation of (A) Th and (B) DBT over (a) TS-1, (b) TS-1@H-mTi-SiO<sub>2</sub> and (c) blank run

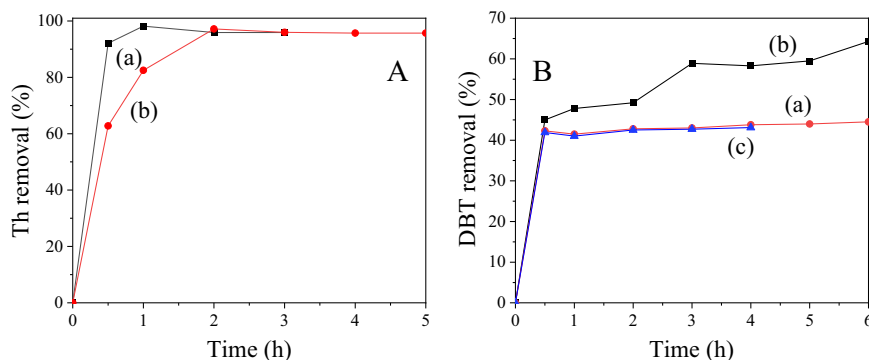
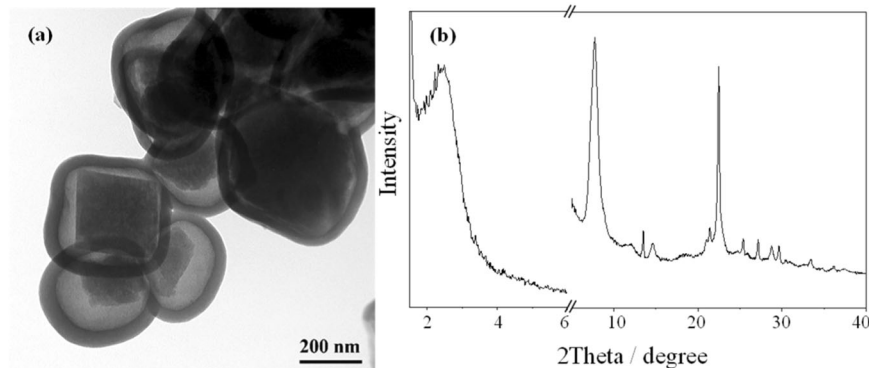


**Fig. 14** TEM image (a) and XRD pattern (b) of H-β@H-mAl-SiO<sub>2</sub>



and zeolite@mSiO<sub>2</sub> micro/mesoporous composites are fabricated and catalytic tested, which provide valuable idea for the design of desired catalytic system to meet the demand of specific reactions.

**Acknowledgements** The authors gratefully acknowledge the financial supports from the Talent Scientific Research Fund of LNPU (2020XJL-016), the Liaoning Provincial Natural Science Foundation of China (2019-MS-323).

**Author contributions** This manuscript was written through contributions from all authors. HL and CJ wrote the main manuscript text. HL and WX finished the preparation experiment. MZ and JX finished characterization and catalytic tests. RW and HJ participated in the discussion and analysis of experiment results. All authors reviewed the manuscript and approved the final version.

## Compliance with ethical standards

**Conflict of interest** The authors declare no competing interests.

## References

- Gawande MB, Goswami A, Asefa T et al. (2015) Core-shell nanoparticles: synthesis and applications in catalysis and electrocatalysis. *Chem Soc Rev* 44:7540–7590. <https://doi.org/10.1039/c5cs00343a>
- Tubtimkuna S, Danilov, DL, Sawangphruk, M et al. (2023) Review of the Scalable Core-Shell Synthesis Methods: The Improvements of Li-Ion Battery Electrochemistry and Cycling Stability. *Small Methods*. <https://doi.org/10.1002/smt.202300345>
- Li ZW, Li M, Bian ZF et al. (2016) Design of highly stable and selective core/yolk-shell nanocatalysts-A review. *Appl Catal B-Environ* 188:324–341. <https://doi.org/10.1016/j.apcatb.2016.01.067>
- Moon GD (2020) Yolk Shell Nanostructures: Syntheses and Applications for Lithium-Ion Battery Anodes. *Nanomaterials-Basel* 10. ARTN 67510.3390/nano10040675
- Dai CY, Zhang AF, Liu M et al. (2015) Hollow ZSM-5 with Silicon-Rich Surface, Double Shells, and Functionalized Interior with Metallic Nanoparticles and Carbon Nanotubes. *Adv Funct Mater* 25:7479–7487. <https://doi.org/10.1002/adfm.201502980>
- Das S, Perez-Ramirez J, Gong JL et al. (2020) Core-shell structured catalysts for thermocatalytic, photocatalytic, and electrocatalytic conversion of CO<sub>2</sub>. *Chem Soc Rev* 49:2937–3004. <https://doi.org/10.1039/c9cs00713j>
- Jin CZ, Wang YJ, Tang HL et al. (2016) Versatile rattle-type magnetic mesoporous silica spheres, working as adsorbents and nanocatalyst containers. *J Sol-Gel Sci Techn* 77:279–287. <https://doi.org/10.1007/s10971-015-3830-1>
- Zhu YF, Ikoma T, Hanagata N et al. (2010) Rattle-type Fe<sub>3</sub>O<sub>4</sub>@-SiO<sub>2</sub> hollow mesoporous spheres as carriers for drug delivery. *Small* 6:471–478. <https://doi.org/10.1002/sml.200901403>
- Chen Y, Chen HR, Guo LM et al. (2010) Hollow/rattle-type mesoporous nanostructures by a structural difference-based selective etching strategy. *ACS Nano* 4:529–539. <https://doi.org/10.1021/nn901398j>
- Dong C, Yu Q, Ye RP et al. (2020) Hollow carbon sphere nanoreactors loaded with pdcu nanoparticles: void-confinement effects in liquid-phase hydrogenations. *Angew Chem Int Ed* 59:18374–18379. <https://doi.org/10.1002/anie.202007297>
- Du D, Shi W, Wang LZ et al. (2017) Yolk-shell structured Fe<sub>3</sub>O<sub>4</sub>@void@TiO<sub>2</sub> as a photo-Fenton-like catalyst for the extremely efficient elimination of tetracycline. *Appl Catal B-Environ* 200:484–492. <https://doi.org/10.1016/j.apcatb.2016.07.043>
- Kuo CH, Tang Y, Chou LY et al. (2012) Yolk-shell nanocrystal@ZIF-8 nanostructures for gas-phase heterogeneous catalysis with selectivity control. *J Am Chem Soc* 134:14345–14348. <https://doi.org/10.1021/ja306869j>
- Lee I, Joo JB, Yin YD et al. (2011) A yolk@shell nanoarchitecture for Au/TiO<sub>2</sub> catalysts. *Angew Chem Int Ed* 50:10208–10211. <https://doi.org/10.1002/anie.201007660>
- Li A, Zhu WJ, Li CC et al. (2019) Rational design of yolk-shell nanostructures for photocatalysis. *Chem Soc Rev* 48:1874–1907. <https://doi.org/10.1039/c8cs00711j>
- Lin LS, Song, JB, Yang, HH et al. (2018) Yolk-shell nanostructures: design, synthesis, and biomedical applications. *Adv Mater* 30. ARTN 170463910.1002/adma.201704639
- Yang Y, Liu X, Li XB et al. (2012) A yolk-shell nanoreactor with a basic core and an acidic shell for cascade reactions. *Angew Chem Int Ed* 51:9164–9168. <https://doi.org/10.1002/anie.201204829>
- Zhao LZ, Peng JJ, Huang Q et al. (2014) Near- infrared photo-regulated drug release in living tumor tissue via yolk-shell upconversion nanocages. *Adv Funct Mater* 24:363–371. <https://doi.org/10.1002/adfm.201302133>
- Qiao MT, Lei XF, Ma Y et al. (2018) Application of yolk-shell Fe<sub>3</sub>O<sub>4</sub>@N-doped carbon nanochains as highly effective microwave-absorption material. *Nano Res* 11:1500–1519. <https://doi.org/10.1007/s12274-017-1767-0>
- Liu J, Qiao SZ, Chen JS et al. (2011) Yolk/shell nanoparticles: new platforms for nanoreactors, drug delivery and lithium-ion batteries. *Chem Commun* 47:12578–12591. <https://doi.org/10.1039/c1cc13658e>
- Zhu T, Zhu LL, Wang J et al. (2016) Rational integration of inbuilt aperture with mesoporous framework in unusual asymmetrical yolk-shell structures for energy storage and conversion. *ACS Appl Mater Inter* 8:32901–32909. <https://doi.org/10.1021/acsami.6b12284>
- Chen JC, Xue ZT, Feng SS et al. (2014) Synthesis of mesoporous silica hollow nanospheres with multiple gold cores and catalytic activity. *J Colloid Inter Sci* 429:62–67. <https://doi.org/10.1016/j.jcis.2014.05.005>
- Chen Z, Cui ZM, Niu F et al. (2010) Pd nanoparticles in silica hollow spheres with mesoporous walls: a nanoreactor with extremely high activity. *Chem Commun* 46:6524–6526. <https://doi.org/10.1039/c0cc01786h>
- Cui ZM, Chen Z, Cao CY et al. (2013) A yolk-shell structured Fe<sub>2</sub>O<sub>3</sub>@mesoporous SiO<sub>2</sub> nanoreactor for enhanced activity as a Fenton catalyst in total oxidation of dyes. *Chem Commun* 49:2332–2334. <https://doi.org/10.1039/c3cc38649j>
- Park JC, Bang JU, Lee J et al. (2010) Ni@SiO<sub>2</sub> yolk-shell nanoreactor catalysts: High temperature stability and recyclability. *J Mater Chem* 20:1239–1246. <https://doi.org/10.1039/b918446e>
- Park JC, Song H (2011) Metal@silica yolk-shell nanostructures as versatile bifunctional nanocatalysts. *Nano Res* 4:33–49. <https://doi.org/10.1007/s12274-010-0039-z>
- Yao TJ, Cui TY, Fang X et al. (2013) Preparation of yolk-shell Fe<sub>x</sub>O<sub>y</sub>/Pd@mesoporous SiO<sub>2</sub> composites with high stability and their application in catalytic reduction of 4-nitrophenol. *Nanoscale* 5:5896–5904. <https://doi.org/10.1039/c3nr01470c>
- Zhang T, Ge J, Hu Y et al. (2008) Formation of hollow silica colloids through a spontaneous dissolution-regrowth process. *Angew Chem Int Ed* 47:5806–5811. <https://doi.org/10.1002/anie.200800927>
- Zhao XY, Li HR, Zhang JP et al. (2016) Design and synthesis of NiCe@m-SiO<sub>2</sub> yolk-shell framework catalysts with improved

- coke- and sintering-resistance in dry reforming of methane. *Int J Hydrog Energy* 41:2447–2456. <https://doi.org/10.1016/j.ijhydene.2015.10.111>
29. Yue Q, Li JL, Zhang Y et al. (2017) Plasmolysis-inspired nanoengineering of functional yolk-shell microspheres with magnetic core and mesoporous silica shell. *J Am Chem Soc* 139:15486–15493. <https://doi.org/10.1021/jacs.7b09055>
30. Wang SN, Zhang MC, Zhang WQ (2011) Yolk-shell catalyst of single au nanoparticle encapsulated within hollow mesoporous silica microspheres. *Acs Catal* 1:207–211. <https://doi.org/10.1021/cs1000762>
31. Wu X-J, Xu D (2009) Formation of yolk/SiO<sub>2</sub> shell structures using surfactant mixtures as template. *J Am Chem Soc* 131:2774–2775. <https://doi.org/10.1021/ja808452r>
32. Wong YJ, Zhu L, Teo WS et al. (2011) Revisiting the Stöber method: in homogeneity in silica shells. *J Am Chem Soc* 133:11422–11425. <https://doi.org/10.1021/ja203316q>
33. Zhang Q, Zhang T, Ge J et al. (2008) Permeable silica shell through surface-protected etching. *Nano Lett* 8:2867–2871. <https://doi.org/10.1021/nl8016187>
34. Liu J, Qiao SZ, Liu H et al. (2011) Extension of the Stöber method to the preparation of monodisperse resorcinol-formaldehyde resin polymer and carbon spheres. *Angew Chem Int Ed* 50:5947–5951. <https://doi.org/10.1002/anie.201102011>
35. Liu R, Qu FL, Guo YL et al. (2014) Au@carbon yolk-shell nanostructures via one-step core-shell-shell template. *Chem Commun* 50:478–480. <https://doi.org/10.1039/c3cc47050d>
36. Fang XL, Liu SJ, Zang J et al. (2013) Precisely controlled resorcinol-formaldehyde resin coating for fabricating core-shell, hollow, and yolk-shell carbon nanostructures. *Nanoscale* 5:6908–6916. <https://doi.org/10.1039/c3nr01723k>
37. Li N, Zhang Q, Liu J et al. (2013) Sol-gel coating of inorganic nanostructures with resorcinol-formaldehyde resin. *Chem Commun* 49:5135–5137. <https://doi.org/10.1039/c3cc41456f>
38. Jin CZ, Wang YJ, Tang HL et al. (2014) Synthesis, characterization, and catalytic applications of core-shell magnetic carbonaceous nanocomposites. *J Phys Chem C* 118:25110–25117. <https://doi.org/10.1021/jp508853a>
39. Wang X, Li SY, Yang GS et al. (2020) Insights into the resorcinol-formaldehyde resin coating process focusing on surface modification of colloidal SiO<sub>2</sub> particles. *Langmuir* 36:2654–2662. <https://doi.org/10.1021/acs.langmuir.9b03595>
40. Thangaraj A, Sivasanker, S (1992) An improved method for TS-1 synthesis - Si-29 NMR-studies. *J Chem Soc-Chem Commun* 123–124. <https://doi.org/10.1039/c39920000123>
41. Fuertes AB, Valle-Vigon P, Sevilla M (2012) One-step synthesis of silica@resorcinol-formaldehyde spheres and their application for the fabrication of polymer and carbon capsules. *Chem Commun* 48:6124–6126. <https://doi.org/10.1039/c2cc32552g>
42. Wang JX, Zhang KM, Kavak S et al. (2023) Modifying the Stöber process: is the organic solvent indispensable? *Chem-Eur J* 29. <https://doi.org/10.1002/chem.202202670>
43. Peyrovi MH, Parsafard N, Anajafi HR (2018) Catalytic performance of micro-mesoporous materials as the supports for Pt catalysts in n-heptane isomerization. *Chem Phys Lett* 713:32–38. <https://doi.org/10.1016/j.cplett.2018.10.005>
44. Jia LX, Sun XY, Ye XQ et al. (2013) Core-shell composites of USY@Mesosilica: Synthesis and application in cracking heavy molecules with high liquid yield. *Micropor Mesopor Mat* 176:16–24. <https://doi.org/10.1016/j.micromeso.2013.03.029>
45. Peng HG, Xu L, Zhang LY et al. (2012) Synthesis of core-shell structured TS-1@mesocarbon materials and their applications as a tandem catalyst. *J Mater Chem* 22:14219–14227. <https://doi.org/10.1039/c2jm31788e>
46. Srivastava VC (2012) An evaluation of desulfurization technologies for sulfur removal from liquid fuels. *RSC Adv* 2:759–783. <https://doi.org/10.1039/c1ra00309g>
47. Li C, Li D, Zou S et al. (2013) Extraction desulfurization process of fuels with ammonium-based deep eutectic solvents. *Green Chem* 15:2793–2799. <https://doi.org/10.1039/c3gc41067f>
48. Zhang H, Li XP, Zhao RX (2021) Preparation of V<sub>2</sub>O<sub>5</sub>/g-C<sub>3</sub>N<sub>4</sub> catalyst and desulfurization ability in model oil. *J Petrochem Univ* 34:7–14. <https://doi.org/10.3969/j.issn.1006-396X.2021.01.002>

**Publisher's note** Springer Nature remains neutral with regard to jurisdictional claims in published maps and institutional affiliations.

Springer Nature or its licensor (e.g. a society or other partner) holds exclusive rights to this article under a publishing agreement with the author(s) or other rightsholder(s); author self-archiving of the accepted manuscript version of this article is solely governed by the terms of such publishing agreement and applicable law.